Superconductivity and non-Fermi liquid behavior near antiferromagnetic quantum critical points in $CeRh_{1-x}Co_xIn_5$

J. R. Jeffries, N. A. Frederick, E. D. Bauer,* Hikari Kimura,† V. S. Zapf,* K.-D. Hof,‡ T. A. Sayles, and M. B. Maple
Department of Physics and Institute for Pure and Applied Physical Sciences, University of California—San Diego, La Jolla, California 92093, USA

(Received 25 January 2005; revised manuscript received 25 April 2005; published 29 July 2005)

Single crystals of $CeRh_{1-x}Co_xIn_5$ have been investigated by means of specific heat measurements at zero pressure and electrical resistivity measurements under nearly hydrostatic pressure up to 28 kbar. Specific heat measurements for samples of $CeRh_{1-x}Co_xIn_5$ with cobalt concentrations of $x=0.65$, 0.71, 0.77, 0.87, and 0.93 confirm the existence of antiferromagnetism for $0\leqslant x\leqslant 0.7$ and suggest the existence of a quantum critical point at $x_c\sim 0.75$. Entropy versus x isotherms below ~ 5 K and the normalized residual resistivity $\rho(0\text{ K})/\rho(290\text{ K})$ versus x curve both display maxima near $x_c\sim 0.75$, suggesting further evidence for the existence and location of the quantum critical point. Electrical resistivity measurements under pressure for samples with $x=0.1$, 0.2, 0.4, and 0.6 reveal antiferromagnetism, pressure-induced superconductivity, and the coexistence of antiferromagnetism and superconductivity. Normalized residual resistivity $\rho(0\text{ K})/\rho(290\text{ K})$ versus pressure P curves and the evolution of the power-law exponent n favor the existence of quantum critical points at critical pressures $P_c\sim 23$ kbar, ~ 21 kbar, and ~ 7 kbar for samples with $x=0.1$, 0.2, and 0.4, respectively.

DOI: 10.1103/PhysRevB.72.024551 PACS number(s): 71.27.+a, 74.62.Fj, 75.50.Ee

I. INTRODUCTION

Since the early 1990s, there has been a growing interest in the breakdown of Fermi liquid theory near quantum critical points (QCPs) in strongly correlated f-electron materials.[1–6] This breakdown is manifested in low-temperature physical properties, such as electrical resistivity, specific heat, and magnetic susceptibility that exhibit weak power law or logarithmic divergences in temperature, commonly referred to as non-Fermi liquid (NFL) behavior. In many of these f-electron materials, the QCP is associated with a second-order phase transition (usually, magnetic) that is suppressed toward 0 K as a function of a control parameter, such as chemical composition, pressure, or magnetic field. However, before the QCP is reached, other phenomena, such as superconductivity coexisting with magnetism[7–10] and short-range or glassy types of magnetic order[11–15] are often observed. As a result of their sensitivity to control parameters, heavy fermion systems are excellent candidates for the investigation of low-temperature properties near a QCP.

A set of heavy fermion compounds structurally related to $CeIn_3$ with the formula $Ce_nT_mIn_{3n+2m}$ (T=Co, Rh, Ir; $n=1,2$; $m=0,1$) was recently discovered and found to exhibit superconductivity (SC), antiferromagnetism (AFM), NFL behavior, and the coexistence of SC and AFM.[16,17] The $CeTIn_5$ compounds can be viewed as alternating layers of the parent compound, $CeIn_3$, and TIn_2 stacked along the c axis. Under ambient pressure, $CeRhIn_5$ evinces AFM at $T_N=3.8$ K,[16] while $CeIrIn_5$ exhibits bulk SC at $T_c=0.4$ K,[18] and $CeCoIn_5$ displays SC at $T_c=2.3$ K, the highest T_c of any Ce-based heavy fermion superconductor.[19] With applied pressure, superconductivity in $CeRhIn_5$ develops out of a non-Fermi liquid normal state above 16.3 kbar.[20] Superconductivity is seen to increase with pressure up to ~ 30 kbar, followed by a decrease and the eventual suppression of superconductivity at a pressure of ~ 85 kbar.[21] Superconductivity in $CeCoIn_5$ also develops out of a non-Fermi liquid normal state, but unlike $CeRhIn_5$, exists at ambient pressure. As pressure is applied to $CeCoIn_5$, T_c increases slightly until ~ 15 kbar, shortly after which normal state Fermi liquid behavior is recovered, followed by a decrease and the eventual suppression of superconductivity at ~ 37 kbar.[22]

Previous ambient pressure electrical resistivity measurements on $CeRh_{1-x}Co_xIn_5$ revealed antiferromagnetic transitions for $0\leqslant x\leqslant 0.4$, and superconducting transitions for $0.4\leqslant x\leqslant 1$.[23] Peaks observed in the specific heat $C(T)$ divided by temperature T, $C(T)/T$, were attributed to AFM for $x\leqslant 0.6$ and superconductivity for $x\geqslant 0.4$. The intermediate region with $0.4\leqslant x\leqslant 0.6$ shows two distinct peaks corresponding to both antiferromagnetism and superconductivity, suggesting the coexistence of both phenomena. Previous measurements of the electronic specific heat coefficient $\gamma\equiv C(T)/T$ imply heavy electron masses, and entropy calculations suggest that in the region of coexistence the same heavy electrons participate in both superconductivity and antiferromagnetism.[23]

In this paper, we report the results of our recent hydrostatic pressure and specific heat studies of $CeRh_{1-x}Co_xIn_5$ emphasizing the existence of and behavior near quantum critical points in both T-P and T-x planes. The correlation between the disappearance of magnetic order and the appearance of superconductivity in some heavy fermion materials has given rise to a magnetic interaction scenario in which spin fluctuations rather than phonons are responsible for the binding of quasiparticles into Cooper pairs. This interaction would likely lead to the existence of superconductivity only over a narrow lattice parameter range in the vicinity of the QCP, as seen in $CeIn_3$ under hydrostatic pressure.[8] The results of our studies on $CeRh_{1-x}Co_xIn_5$ show that, unlike $CeIn_3$, SC exists over a wide range of pressure and concen-

tration, implying a more complex origin of superconductivity in this system.

II. EXPERIMENTAL DETAILS

The $CeRh_{1-x}Co_xIn_5$ single crystals were grown using a molten indium flux technique in alumina crucibles sealed in evacuated quartz tubes. The $x=0.1$ and 0.2 crystals used for electrical resistivity measurements and the $x=0.65$, 0.71, 0.77, 0.87, and 0.93 crystals used for specific heat measurements were grown using the same methods previously reported.[23] The $x=0.4$ crystals were soaked at 1100 °C for 24 h, while the $x=0.6$ crystals were soaked at 1100 °C for only 1 h. Both concentrations were then cooled at 20 °C/h to 750 °C followed by a slower cooling at 5 °C/h to 450 °C, at which point the molten indium flux was spun off in a centrifuge. X-ray powder diffraction measurements indicated that the correct concentrations were obtained, compared to samples previously measured, within experimental error. Single crystals suitable for resistivity measurements typically had sample dimensions of $0.6\times0.6\times1.1$ mm^3.

Electrical contact to the samples was made by attaching four Au wires with Epotek H2OE silver epoxy. Nearly hydrostatic pressure up to 28 kbar was applied to the samples using a beryllium–copper piston-cylinder clamp and a Teflon capsule filled with Fluorinert FC75 as the pressure-transmitting medium. The pressure inside the capsule was determined inductively from the pressure-dependent superconducting transition of a Pb manometer.[24] Four-probe ac electrical resistance measurements from 1 to 300 K were made in a ^{3}He cryostat using a Linear Research LR-201 ac resistance bridge with a frequency of 16 Hz and excitation currents of 1–10 mA. The specific heat C was measured as a function of temperature between 0.6 and 50 K in a ^{3}He semiadiabatic calorimeter by using a standard heat pulse technique.[25] The single crystals (with total masses between 24 and 400 mg) were attached to a sapphire platform with Apiezon N grease.

III. RESULTS

A. Specific heat

Displayed in Fig. 1 are plots of the specific heat divided by temperature $C(T)/T$ versus temperature T for $CeRh_{1-x}Co_xIn_5$ between 0.6 and 6 K. The newly made samples with $x=0.65$, 0.71, 0.77, 0.87, and 0.93 fit in reasonably with the previously measured concentrations.[23] In particular, $x=0.65$ and 0.71 each appear to display the presence of both AFM and SC, although the AFM transition for $x=0.71$ at $T_N=2.1$ K occurs at nearly the same temperature as the SC transition for $x=1$, $CeCoIn_5$. Thus, it is possible that some free $CeCoIn_5$ could instead be the cause of this feature. This possibility was previously noted for $x=0.7$,[23] although for $x=0.71$ the feature is greatly enhanced. Since X-ray results appear to indicate a single phase, it is likely that an AFM transition is actually being observed for $x=0.71$. A phase diagram of the values of T_c and T_N as inferred from the specific heat data is shown in Fig. 5, and will be discussed in a later section.

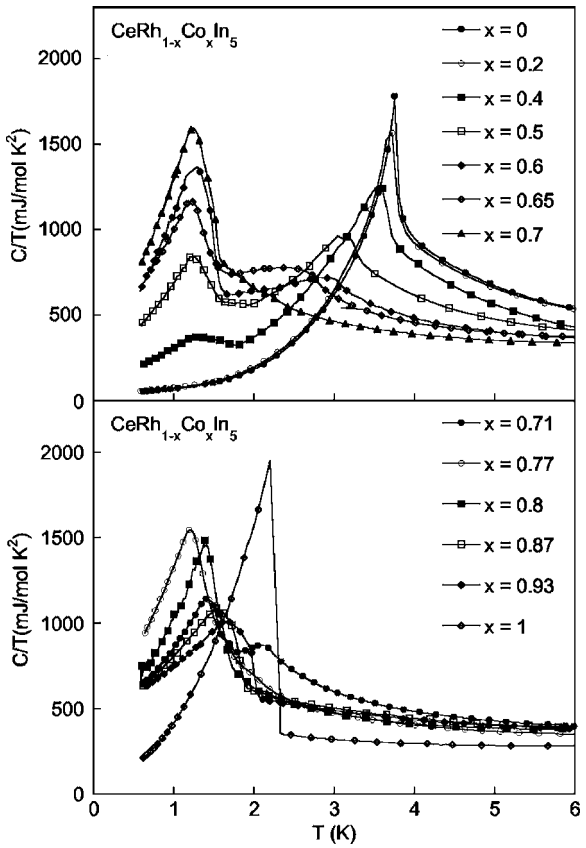

FIG. 1. Specific heat C divided by temperature T, C/T, vs T for $CeRh_{1-x}Co_xIn_5$. In the interest of clarity, the data for the different concentrations are split into two graphs.

The thermodynamic properties of the $CeRh_{1-x}Co_xIn_5$ system obtained from specific heat are summarized in Table I. The superconducting specific heat jump, ΔC, was extracted from the data by assuming an ideal entropy conserving transition. Determining accurate values for the electronic specific heat coefficient γ was difficult due to the presence of the AFM transition in many of the compounds. A detailed description of the process for estimating γ can be found in Zapf *et al.*;[23] a more concise explanation is that for the compounds that display SC, γ was taken as the value of $C(T)/T$ directly above the SC transition, while for the samples which only display AFM behavior, γ was calculated through entropy considerations of the AFM transition. At this time, no definitive conclusion can be drawn from the trends that ΔC and γ follow as a function of x. It should be noted that the estimated values of γ plotted as a function of x appear to display a maximum in the vicinity of $x=0.75$, coincident with the suspected QCP. Since the normal state of $CeCoIn_5$ has been shown to have a temperature-dependent γ when T_c is suppressed to lower temperatures,[19] it is difficult to definitively establish a relationship between the maximum in γ versus x and the QCP without normal state data obtained from specific heat measurements in a magnetic field.

TABLE I. Physical properties of samples of $CeRh_{1-x}Co_xIn_5$, determined from specific heat data. The symbols have the following meanings: T_c—superconducting transition temperature, ΔC—jump in $C(T)$ at T_c, γ—estimated electronic specific heat coefficient, n—power-law exponent of $C(T)/T$ below T_c, and T_N—Néel temperature.

x	T_c (K)	ΔC (mJ/mol K)	γ (mJ/mol K^2)	$\Delta C/\gamma T_c$	n	T_N (K)
0			350			3.8
0.2			340			3.7
0.4	1.5	340	320	0.7	1.57	3.6
0.5	1.4	580	580	0.7	1.63	3.2
0.6	1.43	1560	620	1.8	1.62	2.9
0.65	1.38	930	730	0.9	1.40	2.4
0.7	1.42	1540	820	1.3	1.59	
0.71	1.56	820	830	0.4	1.79	2.1
0.77	1.38	1210	780	0.8	1.48	
0.8	1.49	960	720	1.5	1.48	
0.87	1.73	1030	620	0.5	1.43	
0.93	1.89	1090	560	0.5	1.47	
1.0	2.27	3890	350	4.9	2.29	

B. Electrical resistivity under pressure

The electrical resistivity of $CeRh_{1-x}Co_xIn_5$ for $x=0.1$, 0.2, 0.4, and 0.6 is shown in Figs. 2 and 3. At ambient pressure, the $\rho(T)$ data show a weak temperature dependence above ~150 K followed by a rapid decrease, similar to other heavy fermion materials.[26] The $x=0.4$ and 0.6 compounds exhibit pronounced peaks in $\rho(T)$, due to the onset of coherent scattering of electrons by the Ce ion sublattice,[23] at a characteristic temperature $T^* \approx 17$ K and 27 K, respectively. These peaks, and the subsequent rapid decrease in $\rho(T)$, are similar to those of the end member compound $CeCoIn_5$. The $x=0.1$ and 0.2 compounds do not exhibit peaks, but $\rho(T)$ rapidly decreases below ~32 K and ~40 K, respectively, similar to the other end member compound $CeRhIn_5$. In the $x=0.1$ and 0.2 compounds, the $\rho(T)$ curves display kinks corresponding to the onset of antiferromagnetic order at a Néel temperature $T_N=3.68$ K and 3.50 K, respectively, while the $x=0.4$ compound shows AFM order at $T_N=2.55$ K and SC at $T_c=1.43$ K and the $x=0.6$ compound displays only SC at $T_c=1.89$ K.

With applied pressure, the $x=0.4$ and 0.6 compounds show a broadening of the coherence peaks with little change in the maximum value of $\rho(T)$ at T^*, defined as ρ^*. The aforementioned concentrations exhibit a monotonic increase in T^* up to ~75 K and ~85 K, respectively. The $x=0.1$ and 0.2 compounds develop peaks at T^*, which broaden with pressure, and T^* is seen to first decrease with pressure to a minimum value at ~12 kbar and then increase to ~37 K and ~30 K, respectively; this behavior is similar to that observed for pure $CeRhIn_5$.[20] Since $T^* \propto T_{sf} \propto 1/\gamma$, where T_{sf} is the characteristic spin-fluctuation temperature,[27] the pressure dependence of T^* for the low Co concentration samples is consistent with the pressure dependence of γ in $CeRhIn_5$.[28] While ρ^* increases monotonically with pressure for $x=0.1$, it increases to a maximum at ~17 kbar and then decreases for $x=0.2$. The values of T^* as a function of pressure for the four concentrations are displayed in Fig. 4.

Antiferromagnetic order was no longer detectable at the lowest pressure achieved in the $x=0.4$ compound. As pressure was increased, T_c increased up to 1.61 K at 12.1 kbar

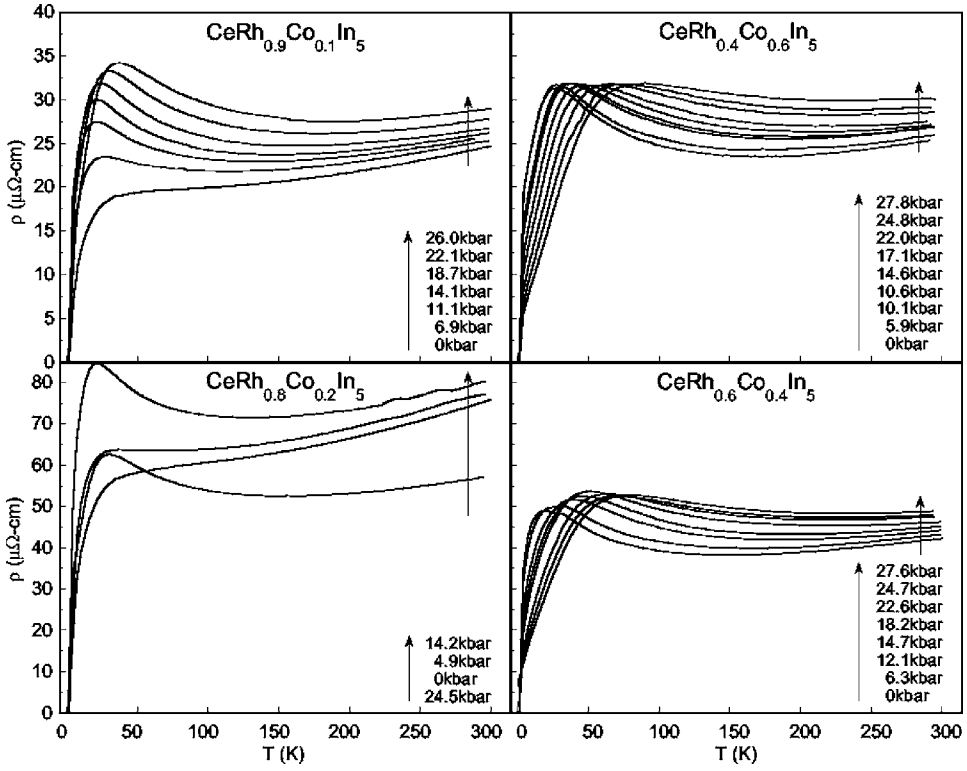

FIG. 2. Electrical resistivity ρ as a function of temperature T for $x=0.1, 0.2, 0.4$, and 0.6 at various pressures.

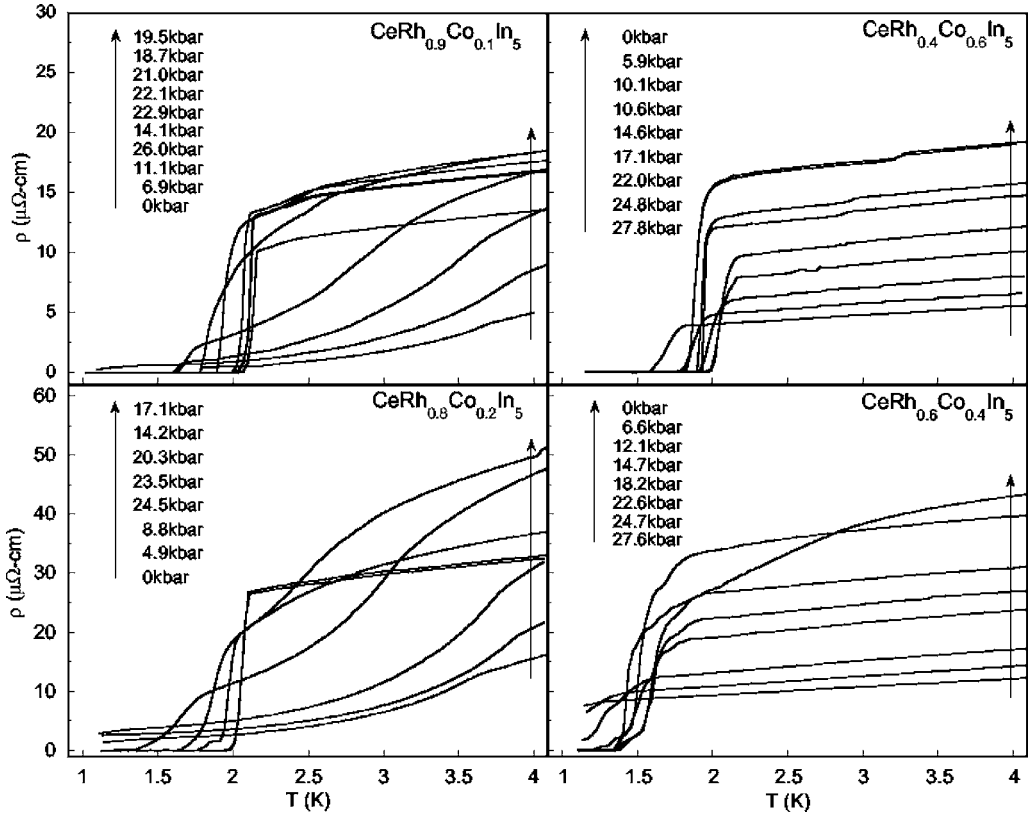

FIG. 3. Low-temperature electrical resistivity ρ as a function of temperature T for $x=0.1, 0.2, 0.4$, and 0.6 at various pressures. AFM can be seen for $x=0.1, 0.2$, and 0.4 and was determined by the inflection point in $\rho(T)$. Superconducting transitions can be seen in all concentrations. The step in $\rho(T)$ under ambient pressure for $x=0.6$ at $T\sim 3.4$ K is attributed to the superconducting transition of free indium.

and 2.05 K at 14.6 kbar for $x=0.4$ and 0.6, respectively. For both concentrations, T_c decreases for pressures in excess of those at which T_c is a maximum and the superconducting transitions broaden with increasing pressure.

For specimens with $x=0.1$ and 0.2, T_N increased slightly for low pressure, then fell off as pressure was increased until it could no longer be detected. SC was detected at 6.9 kbar with a T_c of 1.11 K and at 8.8 kbar with an estimated T_c of 0.82 K, respectively. The onset of SC was not observed above 1 K for pressures below 6.9 kbar and 8.8 kbar in samples with $x=0.1$ and 0.2, respectively. As pressure was increased, T_c increased monotonically for samples with $x=0.1$ and 0.2 to a value of 2.12 K at 26 kbar and 2.05 K at 24.5 kbar, respectively. The superconducting transition widths for both concentrations narrowed with increasing pressure.

IV. DISCUSSION

A. Specific heat and electrical resistivity at zero pressure

The revised T-x phase diagram is shown in Fig. 5. Because specific heat is a more reliable probe than electrical resistivity for the bulk superconducting and antiferromagnetic transitions that occur in $CeRh_{1-x}Co_xIn_5$, only specific heat data from this study and the previous specific heat study by Zapf *et al.*[23] are included in Fig. 5. The new data fit in well with the previous data. The data from this study show more detail in the region of the suspected QCP, verifying that the Néel temperature indeed falls off toward zero temperature above $x=0.6$. In addition, the new concentrations have filled in the region in concentration between the QCP and pure $CeCoIn_5$, revealing that the suppression of T_c is indeed arrested by the onset of antiferromagnetic order at $x\sim 0.7$.

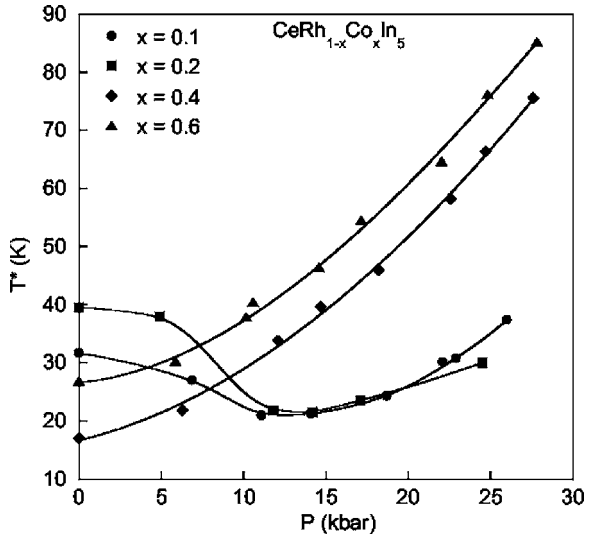

FIG. 4. The values of T^* as a function of pressure for $x=0.1, 0.2, 0.4$, and 0.6. The solid lines are guides for the eyes.

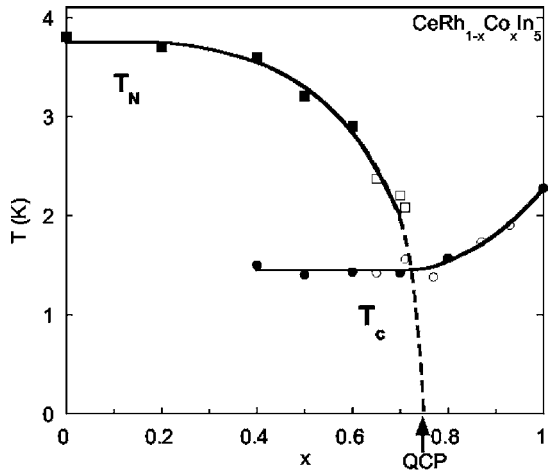

FIG. 5. Temperature T vs Co concentration x phase diagram for $CeRh_{1-x}Co_xIn_5$. Only the Néel temperatures T_N and superconducting critical temperatures T_c determined from specific heat $C(T)$ are displayed. Closed symbols indicate data from Zapf *et al.* (Ref. 23). Open symbols indicate data from the current study. The lines are guides for the eyes.

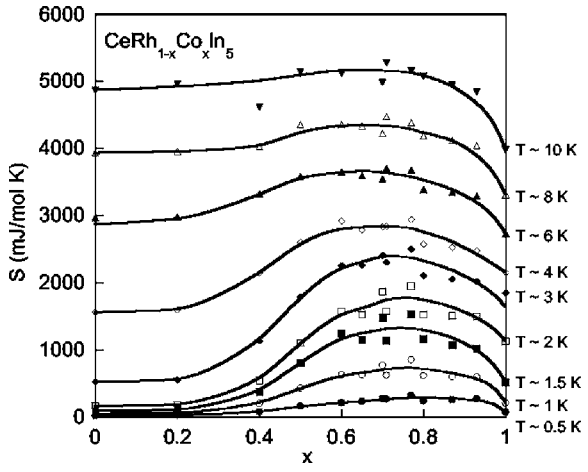

FIG. 6. Isotherms of entropy S vs Co concentration x for $CeRh_{1-x}Co_xIn_5$. The entropy is noticeably enhanced at lower temperatures near the suspected QCP at $x \sim 0.75$.

In order to calculate the entropy of the $CeRh_{1-x}Co_xIn_5$ system, the $C(T)$ data below T_c were fit by the relation $C(T)=AT+BT^{n+1}$, corresponding to the more familiar relation for unconventional superconductivity, $C(T)/T=A+BT^n$. The values of n calculated with this method are listed in Table I. The exponent n varies only slightly between 1.4 and 1.8 for all superconducting concentrations up to $x=1$, $CeCoIn_5$, where it jumps up to a value of 2.3. The new concentrations, in general, continue the trend observed previously,[23] indicating non-s-wave pairing. Several of the new samples have values of $n \sim 1.4-1.5$ which are not consistent with the prediction of $n=2$ for a superconducting gap which vanishes at lines on the Fermi surface.[29] With these additional data, the previous samples also appear to disagree with these theories. At present, because of the likely temperature dependence of γ, these values of n will have to be taken as approximations, useful mostly for extrapolating the data to 0 K in order to estimate the entropy. Furthermore, the power-law dependence of the physical properties in the superconducting state, indicative of nodes in the superconducting energy gap, is only expected to be valid for temperature $T \ll T_c$, although power-law temperature dependencies of $C(T)$ within the superconducting state from $T \ll T_c$ up to temperatures comparable to T_c have been observed in several heavy fermion superconductors including $CeCu_2Si_2$ and URu_2Si_2.[30,31]

The entropy data for the new $CeRh_{1-x}Co_xIn_5$ samples are similar to those previously measured.[23] The calculated S versus T curves are not repeated here in the interest of brevity. However, it was discovered that plotting isotherms of S as a function of Co concentration x revealed an enhancement near $x \simeq 0.75$. These isotherms below 10 K are shown in Fig. 6. The presence of this increased entropy around the concentration where a QCP is suspected reveals the presence of low-lying excitations and adds further support to this hypothesis. Around $T=6$ K, the entropy is nearly constant, with the exception of $CeCoIn_5$. This could suggest the presence of antiferromagnetic order due to the small Rh concentration of the samples with $x=0.8$, 0.87, and 0.93. The similar entropy at $T=0.5$ K and 1 K also suggests that similar mechanisms are at work below T_c in all the samples which display SC, both above and below the suspected QCP. Whether or not there is a full AFM transition below T_c remains to be seen, and would require measurements of C to temperatures below and magnetic fields above those achievable in our experimental setup ($\sim$0.4 K and 6 T).

The presence of a QCP is also supported by the electrical resistivity data near $x \simeq 0.75$. Peaks in residual resistivity versus a tuning parameter, such as pressure or concentration, often occur in the region of the QCP.[32–34] Here, normalized electrical residual resistivity, $\rho(0\ \mathrm{K})/\rho(290\ \mathrm{K})$, is used to eliminate the error in resistivity due to determining the geometrical factor of the sample. Figure 7 shows the normalized residual resistivity versus x for $CeRh_{1-x}Co_xIn_5$, which displays a pronounced peak in the vicinity of $x \simeq 0.75$, the QCP in the T-x phase diagram. The presence of low-lying excitations inferred from the peak in S versus x isotherms at low temperatures is consistent with the increased scattering im-

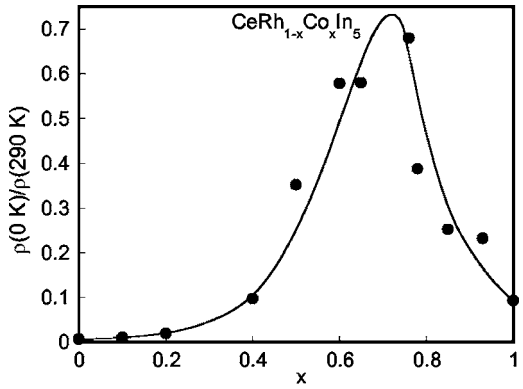

FIG. 7. Normalized residual resistivity $\rho(0\ \mathrm{K})/\rho(290\ \mathrm{K})$ as a function of Co concentration x at ambient pressure. The solid line is a guide to the eyes.

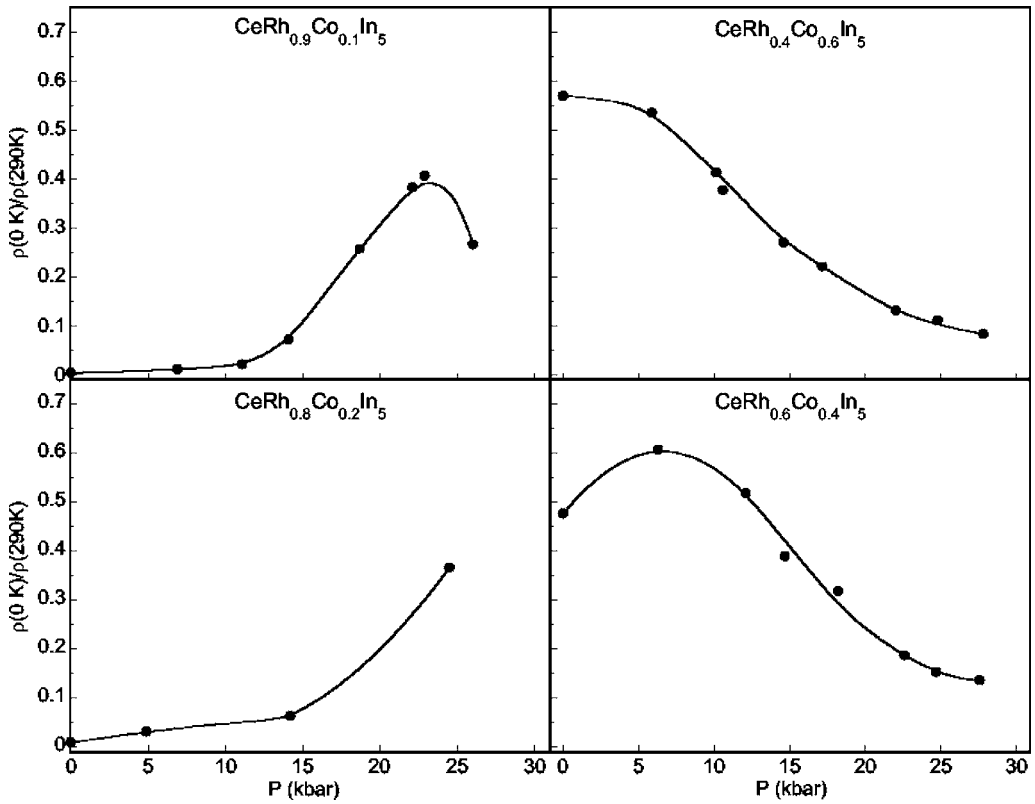

FIG. 8. Normalized residual resistivity $\rho(0\ \mathrm{K})/\rho(290\ \mathrm{K})$ as a function of pressure P for $x=0.1, 0.2, 0.4$, and 0.6. The solid lines are guides for the eyes.

plied by the peak in the normalized residual resistivity versus x curve. This correlation suggests that normalized residual resistivity may be a useful quantity in determining the approximate location of a QCP on the pressure axis for the $CeRh_{1-x}Co_xIn_5$ samples studied under pressure.

B. Electrical resistivity under pressure

Figure 8 shows the normalized residual resistivity versus pressure of $CeRh_{1-x}Co_xIn_5$ for $x=0.1$, 0.2, 0.4, and 0.6 extrapolated from the data shown in Fig. 3. Peaks in $\rho(0\ \mathrm{K})/\rho(290\ \mathrm{K})$ can be distinctly seen for the $x=0.1$ and 0.4 samples at pressures of $\sim$23 kbar and $\sim$7 kbar, respectively. The $x=0.6$ compound shows the tail end of a peak that may occur at $\sim$1 kbar; however, there are insufficient data below 6 kbar to absolutely confirm this statement. The $x=0.2$ compound does not conclusively show a peak below 24 kbar; however, greater pressure or data density could elucidate such a peak. As with the peak in the normalized residual resistivity as a function of x, these peaks as a function of pressure can be used to estimate the location of the QCPs in this system.

The electrical resistivity of $CeRh_{1-x}Co_xIn_5$ sufficiently below the coherence temperature T^* can be described by a power law $\rho-\rho_0=AT^n$. The range of these power-law fits extends down to a temperature just above either the AFM transition or the SC transition. An example of these fits for $x=0.1$ is shown in Fig. 9, a plot of the reduced electrical resistivity $\rho-\rho_0$ versus the reduced temperature $T-T_{N,c}$ on a log-log scale, where $T_{N,c}$ was chosen to be the greater of T_N or T_c. The change in the slope of the fits with increasing pressure indicates a change in the exponent n as a function of pressure. For the concentrations measured, the exponent n was found to be less than the expected Fermi-liquid value of

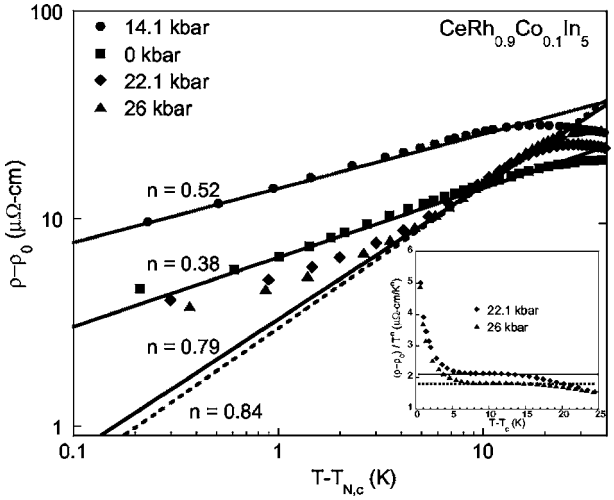

FIG. 9. Low-temperature electrical resistivity of $CeRh_{0.9}Co_{0.1}In_5$ at various pressures plotted as reduced electrical resistivity $\rho-\rho_0$ vs reduced temperature $T-T_{N,c}$ on a log-log plot exemplifying power-law fits of the form $\rho-\rho_0=AT^n$. The solid and dashed lines represent the fits; the dashed line was used for clarity to display the fit for $P=26$ kbar. The change in the exponent n is evinced by the change in slope of the fits. The inset shows $\rho-\rho_0/T^n$ vs $T-T_c$ for $P=22.1$ and 26 kbar. The constant region of the curve indicates the range over which the power-law fit is valid.

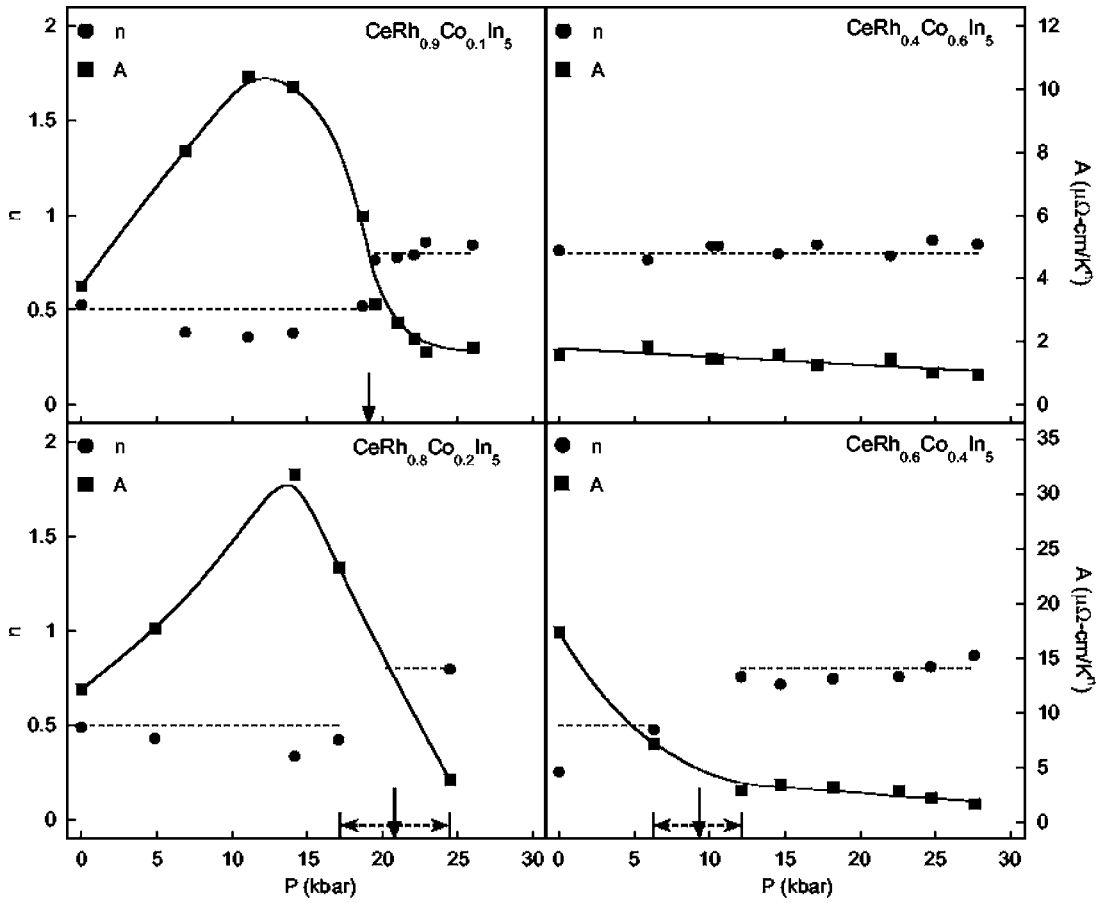

FIG. 10. Values of A and n from power-law fits of the form $\rho-\rho_0=AT^n$ as a function of pressure for $x=0.1, 0.2, 0.4$, and 0.6. The solid and dashed lines are guides for the eyes. The downward pointing arrows indicate an estimate of the pressure at which the exponent n changes, while the dashed, horizontal double-arrows indicate the error in assigning the that pressure.

$n=2$, consistent with other heavy fermion compounds near a QCP, including the parent compound $CeIn_3$.[35] Furthermore, the resistivity was found to vary sublinearly with temperature with the $n<1$ exponent persisting up to the highest pressures achieved. Even at the highest pressures attained in this experiment, there was no evidence indicating a crossover from NFL behavior to the more familiar Fermi liquid behavior as would be expected for pressures in excess of the critical pressure P_c of the QCP.[6]

As shown in Fig. 10, the exponent n ascertained from power-law fits described above displays quantitatively similar behavior as a function of pressure for the four concentrations examined in this study. In the low-pressure region where AFM exists, n assumes a value of $\sim$0.5 or less, while for high pressures, where AFM has been suppressed, n assumes a value of $\sim$0.8. A similar discontinuity in the power-law exponent n was seen in MnSi near the critical pressure at which a ferromagnetic QCP is expected to occur;[36] however, before the ferromagnetic QCP is achieved under pressure, another type of partially ordered magnetic state, associated with the directional freedom of the helical modulation of ferromagnetic order, emerges.[37] While the exponent n in the low-pressure region could be attributed to antiferromagnetic fluctuations, as opposed to NFL behavior, the change in n with increasing pressure nevertheless suggests that the system is in proximity to a QCP. Furthermore, the crossover from low-pressure exponent to high-pressure exponent occurs in the vicinity of the pressures at which the normalized residual resistivity (Fig. 8) exhibit maxima, providing further support for the existence of QCPs in this system.

The values of the coefficient A obtained from the above-mentioned power-law fits are also shown in Fig. 10. These values, like those of the exponent n, display similar behavior for each sample measured, with A approaching 1 $\mu\Omega$ cm/K^n in the pressure region where AFM has been suppressed. For the $x=0.1$ and 0.2 compounds, A exhibits a maximum at $\sim$12 kbar and $\sim$15 kbar, respectively, followed by a rapid decrease with increasing pressure. The $x=0.4$ sample displays a rapid decrease in A at low pressures, where AFM is present, followed by a shallow decrease with increasing pressure. With increasing pressure, the $x=0.6$ specimen shows no rapid decrease in A; instead, it only shows a shallow decrease towards 1 $\mu\Omega$ cm/K^n.

The temperature-pressure (T-P) phase diagrams, determined from resistivity measurements under pressure, are shown in Fig. 11. The Néel temperature T_N is defined as the inflection point in $\rho(T)$, and the QCPs denoted in Fig. 11 are estimated using a combination of the location of the peaks in Fig. 8 and extrapolation of T_N to zero temperature. The superconducting transition temperature T_c is defined as the

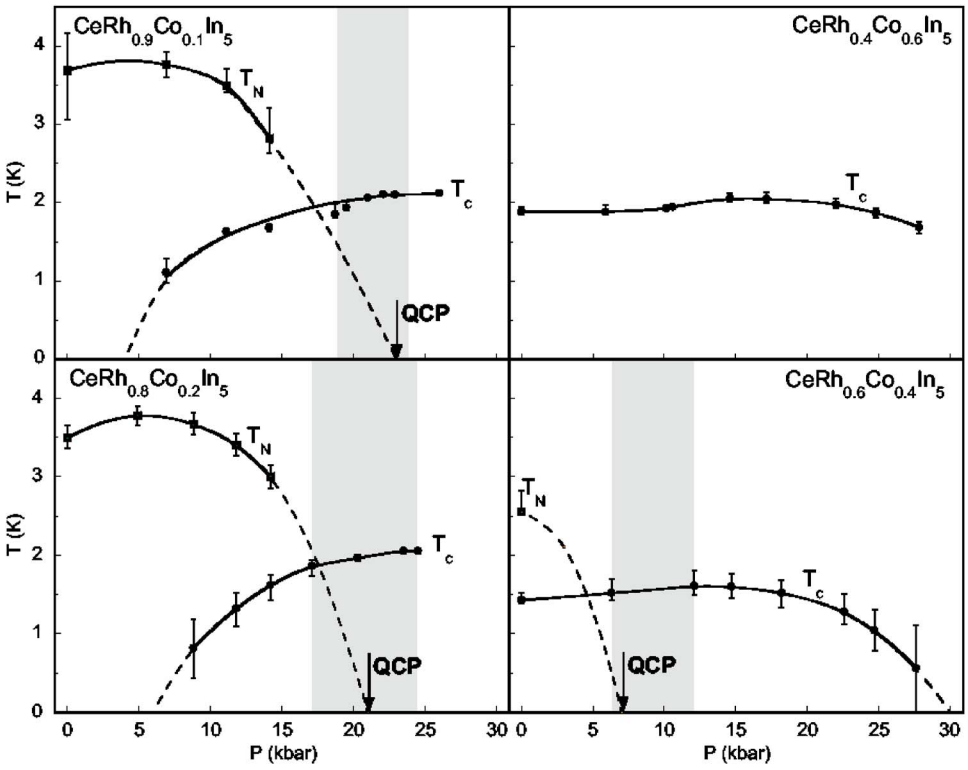

FIG. 11. (Color online) *T-P* phase diagrams for $x=0.1, 0.2, 0.4$, and 0.6 constructed from electrical resistivity data only. The Néel temperature, T_N, is indicated by the filled squares, while the superconducting transition temperature, T_c, is indicated by the filled circles. The value of T_N is taken as the inflection point, determined from the second derivative, of $\rho(T)$ in Fig. 3. The value of T_c is estimated from the midpoint of the zero resistance transition of $\rho(T)$ in Fig. 3. The solid and dashed lines are guides for the eyes, the latter being extrapolations of the data to zero temperature. The downward arrows indicate the QCPs as determined from extrapolation of the Néel temperature combined with the positions of the peaks in the normalized residual resistivity (Fig. 8). The shaded area delineates the region most likely to contain the QCP and was estimated from the uncertainty in the change of n (Fig. 10) and position of the peak in normalized residual resistivity. No signature attributable to AFM was seen in electrical resistivity measurements on the $x=0.6$ sample, therefore, no region of AFM appears in the figure.

temperature at which the resistivity is 50% of the normal state value. For the $x=0.1$ and 0.2 samples, T_N increases slightly, passes through a broad maximum, and then decreases toward 0 K at extrapolated QCPs with critical pressures P_c estimated to be ~ 23 kbar and ~ 21 kbar for $x=0.1$ and 0.2, respectively. The Néel temperature for the $x=0.4$ specimen is quickly suppressed to a QCP at an estimated pressure of ~ 7 kbar. SC is first detected in the $x=0.1$ and 0.2 samples at 6.9 kbar and 8.8 kbar, respectively, where it coexists with AFM with a monotonically increasing T_c until the respective QCP, after which SC persists and T_c continues to increase to the highest pressures. SC exists at ambient pressure in the $x=0.4$ compound and coexists with AFM with an increasing T_c until the QCP, after which T_c continues to increase up to 12.1 kbar followed by a decrease and the eventual destruction of SC at an estimated pressure of ~ 30 kbar. SC exists alone without any evidence of AFM in the $x=0.6$ sample; T_c increases monotonically up to 14.6 kbar followed by a decrease in T_c with pressure. There were insufficient data to extrapolate the pressure at which SC disappears for the $x=0.6$ sample. The monotonically decreasing, concentration-dependent evolution of the QCP $P_c(x)$ is consistent with the existence of the zero-pressure QCP at $x_c \approx 0.75$. This fact, along with the similarities in the behavior of the electrical resistivity in the vicinity of the QCPs, suggests that both pressure and concentration affect the same intrinsic parameter responsible for the quantum critical behavior in this system.

The parent compound of the $CeTIn_5$ compounds, $CeIn_3$, displays SC only over a narrow pressure range of ~ 6 kbar centered about the pressure at which T_c is a maximum. $CeRh_{1-x}Co_xIn_5$, on the other hand, exhibits SC over a broad range of pressure not necessarily centered about the maximum in T_c. This disparity in qualitative features of the phase diagram for $CeIn_3$ and $CeRh_{1-x}Co_xIn_5$ suggests a more complicated origin of SC for the latter system.

V. CONCLUDING REMARKS

Specific heat measurements have revealed more detail in the region of the suspected QCP in the temperature-concentration (T-x) phase diagram of the $CeRh_{1-x}Co_xIn_5$ system, revealing that AFM exists for $0 \leqslant x \leqslant 0.7$. Entropy calculations display a maximum in the isotherms of entropy S versus x at $x \simeq 0.75$, indicative of low-lying excitations near this concentration. The maximum in the S versus x isotherms occurs at the same concentration at which a peak in normalized residual resistivity appears. These observations favor the

existence of a zero-pressure QCP in the vicinity of $x=0.75$. Apparently, antiferromagnetic fluctuations in the vicinity of $x_c \simeq 0.75$ are manifested in the peak in the isotherms of S versus x at low temperature, and the peak in ρ_0 versus x due to the increased electron scattering.

Measurements of electrical resistivity under pressure have been performed on $CeRh_{1-x}Co_xIn_5$ with cobalt concentrations of $x=0.1$, 0.2, 0.4, and 0.6. AFM is suppressed with pressure, and, in the case of the $x=0.1$ and 0.2 compounds, SC appears upon the application of pressure. SC is observed to coexist with AFM from its appearance until a QCP in all concentrations measured except $x=0.6$, for which no AFM signature was seen in the electrical resistivity. SC is also observed over a very wide range of pressure around the QCP, similar to other heavy fermion superconductors,[38] but distinctly unlike $CeIn_3$. The electrical resistivity exhibits NFL behavior with a power-law temperature dependence of the form $\rho-\rho_0=AT^n$ with n displaying a low-pressure value ($n \leqslant 0.5$) associated with the existence of AFM and a distinctly disparate high-pressure value ($n \sim 0.8$) above the pressure at which AFM is destroyed. This NFL behavior occurs over the entire pressure range of the experiment, unlike $CeIn_3$ where NFL behavior only exists in a narrow region around the QCP.[8] There was no evidence for the more familiar T^2 Fermi liquid behavior, even at the highest pressure measured. The location of the QCPs in $CeRh_{1-x}Co_xIn_5$ for $x=0.1$, 0.2, and 0.4 have been estimated at ~ 23 kbar, ~ 21 kbar, and ~ 7 kbar, respectively. The QCP for $x=0.6$ could not be determined, because the electrical resistivity lacked any discernable features that could be attributed to AFM. The evolution of the QCP with chemical substitution suggests that the mechanism at work to produce the quantum critical behavior observed in $CeRh_{1-x}Co_xIn_5$ is affected similarly by both pressure and chemical substitution.

ACKNOWLEDGMENTS

We would like to thank P. Johnson for his assistance with sample synthesis and J. Paglione for fruitful discussions. This research was sponsored by the U. S. Department of Energy under Grant No. DE-FG02-04ER46105, the U. S. National Science Foundation under Grant No. DMR-0335173, and the National Nuclear Security Administration under the Stewardship Science Academic Alliances program through DOE Research Grant No. DE-FG52-03NA00068.

*Permanent address: Los Alamos National Laboratory, Los Alamos, NM 87545, USA.

†Permanent address: Department of Physics, University of California at Berkeley, Berkeley, CA 94720-7300, USA.

‡Permanent address: Universität Karlsruhe, Germany.

[1] C. L. Seaman, M. B. Maple, B. W. Lee, S. Ghamaty, M. S. Torikachvili, J. S. Kang, L. Z. Liu, J. W. Allen, and D. L. Cox, Phys. Rev. Lett. **67**, 2882 (1991).

[2] B. Andraka and A. M. Tsvelik, Phys. Rev. Lett. **67**, 2886 (1991).

[3] H. v. Löhneysen, T. Pietrus, G. Portisch, H. G. Schlager, A. Schröder, M. Sieck, and T. Trappmann, Phys. Rev. Lett. **72**, 3262 (1994).

[4] M. B. Maple, C. L. Seaman, D. A. Gajewski, Y. Dalichaouch, V. B. Barbetta, M. C. de Andrade, H. A. Mook, H. G. Lukefahr, O. O. Bernal, and D. E. MacLaughlin, J. Low Temp. Phys. **95**, 225 (1994).

[5] See various articles in Proceedings of the Institute for Theoretical Physics Conference on Non-Fermi Liquid Behavior in Metals, Santa Barbara, 1996, P. Coleman, M. B. Maple, and A. J. Millis, eds., J. Phys.: Condens. Matter 8 (1996).

[6] G. R. Stewart, Rev. Mod. Phys. **73**, 797 (2001).

[7] F. M. Grosche, S. R. Julian, N. D. Mathur, and G. G. Lonzarich, Physica B **223**, 50 (1996).

[8] F. M. Grosche, I. R. Walker, S. R. Julian, N. D. Mathur, D. M. Freye, M. J. Steiner, and G. G. Lonzarich, J. Phys.: Condens. Matter **13**, 2845 (2001).

[9] S. S. Saxena, P. Agarwal, K. Ahilan, F. M. Grosche, R. K. W. Haselwimmer, M. J. Steiner, E. Pugh, I. R. Walker, S. R. Julian, P. Monthoux, G. G. Lonzarich, A. Huxley, I. Sheikin, D. Braithwaite, and J. Flouquet, Nature (London) **406**, 587 (2000).

[10] E. D. Bauer, R. P. Dickey, V. S. Zapf, and M. B. Maple, J. Phys.: Condens. Matter **13**, L759 (2001).

[11] D. A. Gajewski, N. R. Dilley, R. Chau, and M. B. Maple, J. Phys.: Condens. Matter **8**, 9793 (1996).

[12] D. A. Gajewski, R. Chau, and M. B. Maple, Phys. Rev. B **62**, 5496 (2000).

[13] M. B. Maple, E. D. Bauer, V. S. Zapf, and P.-C. Ho, Physica B **318**, 68 (2002).

[14] V. S. Zapf, R. P. Dickey, E. J. Freeman, C. Sirvent, and M. B. Maple, Phys. Rev. B **65**, 024437 (2001).

[15] R. P. Dickey, E. J. Freeman, V. S. Zapf, P.-C. Ho, and M. B. Maple, Phys. Rev. B **68**, 144402 (2003).

[16] J. D. Thompson, R. Movshovich, Z. Fisk, F. Bouquet, N. J. Curro, R. A. Fisher, P. C. Hammel, H. Hegger, M. F. Hundley, M. Jaime, P. G. Pagliuso, C. Petrovic, N. E. Phillips, and J. L. Sarrao, J. Magn. Magn. Mater. **226**, 5 (2001).

[17] T. Mito, S. Kawasaki, Y. Kawasaki, G.-q. Zheng, Y. Kitaoka, D. Aoki, Y. Haga, and Y. Onuki, Phys. Rev. Lett. **90**, 077004 (2003).

[18] C. Petrovic, R. Movshovich, M. Jaime, P. G. Pagliuso, M. F. Hundley, J. L. Sarrao, Z. Fisk, and J. D. Thompson, Europhys. Lett. **53**, 354 (2001).

[19] C. Petrovic, P. G. Pagliuso, M. F. Hundley, R. Movshovich, J. L. Sarrao, J. D. Thompson, Z. Fisk, and P. Monthoux, J. Phys.: Condens. Matter **13**, L337 (2001).

[20] H. Hegger, C. Petrovic, E. G. Moshopoulou, M. F. Hundley, J. L. Sarrao, Z. Fisk, and J. D. Thompson, Phys. Rev. Lett. **84**, 4986 (2000).

[21] T. Muramatsu, N. Tateiwa, T. C. Kobayashi, K. Shimizu, K. Amaya, D. Aoki, H. Shishido, Y. Haga, and Y. Onuki, J. Phys. Soc. Jpn. **70**, 3362 (2001).

[22] V. A. Sidorov, M. Nicklas, P. G. Pagliuso, J. L. Sarrao, Y. Bang, A. V. Balatsky, and J. D. Thompson, Phys. Rev. Lett. **89**, 157004 (2002).

[23] V. S. Zapf, E. J. Freeman, E. D. Bauer, J. Petricka, C. Sirvent, N. A. Frederick, R. P. Dickey, and M. B. Maple, Phys. Rev. B **65**, 014506 (2001).
[24] T. F. Smith, C. W. Chu, and M. B. Maple, Cryogenics **54**, 53 (1969).
[25] R. Bachmann, F. J. DiSalvo, Jr., T. H. Geballe, R. L. Greene, R. L. Howard, C. N. King, H. C. Kirsch, K. N. Lee, R. E. Schwall, H.-U. Thomas, and R. B. Zubeck, Rev. Sci. Instrum. **43**, 205 (1972).
[26] Z. Fisk, D. W. Hess, C. J. Pethick, D. Pines, J. L. Smith, J. D. Thompson, and J. O. Willis, Science **239**, 33 (1988).
[27] M. Nicklas, R. Borth, E. Lengyel, P. G. Pagliuso, J. L. Sarrao, V. A. Sidorov, G. Sparn, F. Steglich, and J. D. Thompson, J. Phys.: Condens. Matter **13**, 905 (2001).
[28] R. A. Fisher, F. Bouquet, N. E. Phillips, M. F. Hundley, P. G. Pagliuso, J. L. Sarrao, Z. Fisk, and J. D. Thompson, Phys. Rev. B **65**, 224509 (2002).
[29] M. Sigrist and K. Ueda, Rev. Mod. Phys. **63**, 239 (1991).
[30] G. R. Stewart, Rev. Mod. Phys. **56**, 755 (1984).
[31] J. P. Brison, N. Keller, P. Lejay, A. Huxley, L. Schmidt, A. Buzdin, N. R. Bernhoeft, I. Mineev, A. N. Stepanov, J. Flouquet, D. Jaccard, S. R. Julian, and G. G. Lonzarich, Physica B **199**, 70 (1994).
[32] E. D. Bauer, R. P. Dickey, V. S. Zapf, and M. B. Maple, J. Phys.: Condens. Matter **13**, 759 (2001).
[33] V. A. Sidorov, E. D. Bauer, N. A. Frederick, J. R. Jeffries, S. Nakatsuji, N. O. Moreno, J. D. Thompson, M. B. Maple, and Z. Fisk, Phys. Rev. B **67**, 224419 (2003).
[34] D. Jaccard, H. Wilhelm, K. Alami-Yadri, and E. Vargoz, Physica B **259**, 1 (1999).
[35] N. D. Mathur, F. M. Grosche, S. R. Julian, I. R. Walker, R. K. W. Haselwimmer, and G. G. Lonzarich, Nature (London) **394**, 39 (1998).
[36] N. Doiron-Leyraud, I. R. Walker, L. Taillefer, M. J. Steiner, S. R. Julian, and G. G. Lonzarich, Nature (London) **425**, 595 (2003).
[37] C. Pfleiderer, D. Reznik, L. Pintschovius, H. v. Löhneysen, M. Garst, and A. Rosch, Nature (London) **427**, 227 (2004).
[38] F. Thomas, J. Thomasson, C. Ayache, C. Geibel, and F. Steglich, Physica B **186**, 303 (1993).